iScience

CellPress
OPEN ACCESS

Article

CGK733 alleviates ovariectomy-induced bone loss through blocking RANKL-mediated Ca^{2+} oscillations and NF-κB/MAPK signaling pathways

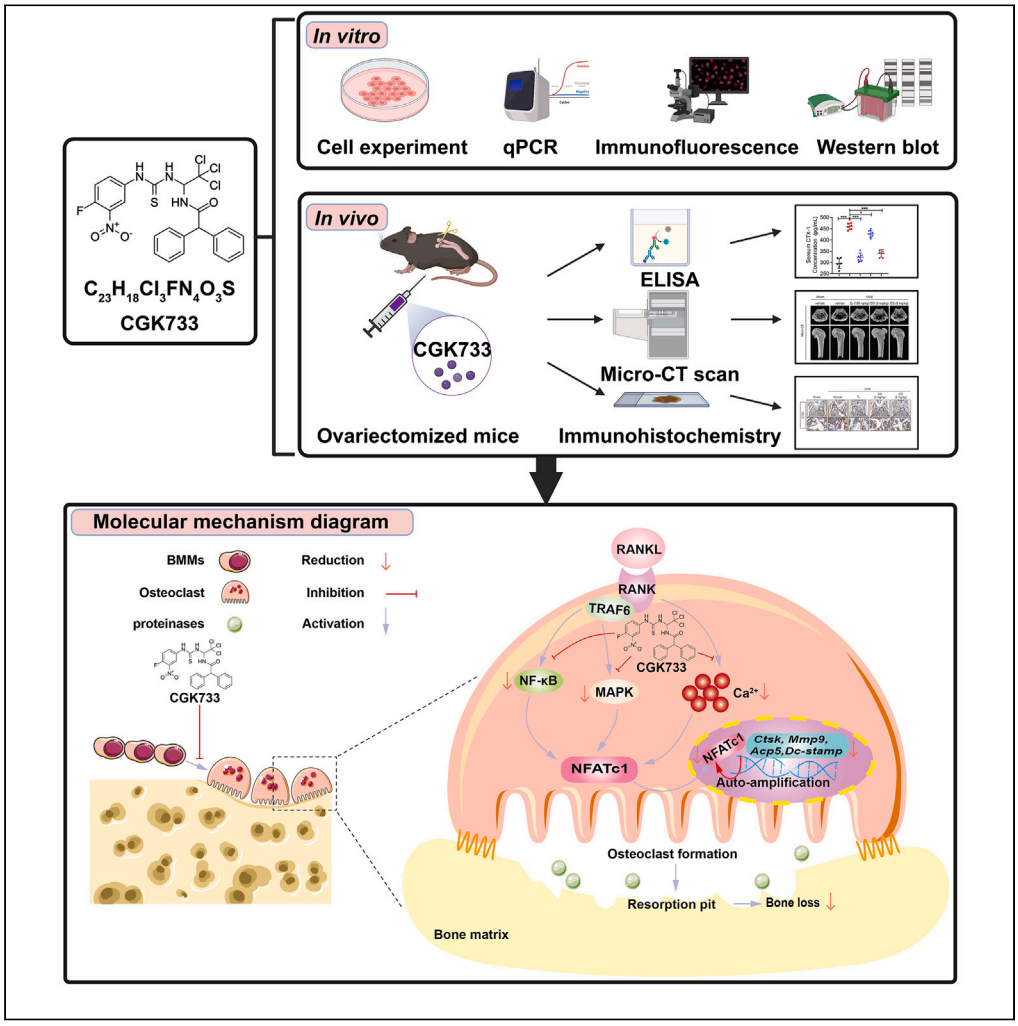

Minglian Xu, Dezhi Song, Xiaoxiao Xie, ..., Jiake Xu, Jinmin Zhao, Qian Liu

liuqian@gxmu.edu.cn (Q.L.)
zhaojinmin@126.com (J.Z.)

Highlights

CGK733 can inhibit osteoclast by blocking Ca^{2+} oscillations and NF-κB/MAPK pathways

CGK733 can alleviate estrogen deficiency-induced bone loss

CGK733 may be a potential drug for the treatment of osteoporosis

Xu et al., iScience 26, 107760
October 20, 2023
https://doi.org/10.1016/j.isci.2023.107760

iScience

CellPress
OPEN ACCESS

Article

CGK733 alleviates ovariectomy-induced bone loss through blocking RANKL-mediated Ca^{2+} oscillations and NF-κB/MAPK signaling pathways

Minglian Xu,[1,2,5] Dezhi Song,[1,2,5] Xiaoxiao Xie,[1,2] Yiwu Qin,[1,2] Jian Huang,[1,2] Chaofeng Wang,[1,2] Junchun Chen,[1,2] Yuangang Su,[1,2] Jiake Xu,[3,4] Jinmin Zhao,[1,2,*] and Qian Liu[1,2,6,*]

SUMMARY

Osteoporosis is a prevalent systemic metabolic disease in modern society, in which patients often suffer from bone loss due to over-activation of osteoclasts. Currently, amelioration of bone loss through modulation of osteoclast activity is a major therapeutic strategy. Ataxia telangiectasia mutated (ATM) inhibitor CGK733 (CG) was reported to have a sensitizing impact in treating malignancies. However, its effect on osteoporosis remains unclear. In this study, we investigated the effects of CG on osteoclast differentiation and function, as well as the therapeutic effects of CG on osteoporosis. Our study found that CG inhibits osteoclast differentiation and function. We further found that CG inhibits the activation of NFATc1 and ultimately osteoclast formation by inhibiting RANKL-mediated Ca^{2+} oscillation and the NF-κB/MAPK signaling pathway. Next, we constructed an ovariectomized mouse model and demonstrated that CG improved bone loss in ovariectomized mice. Therefore, CG may be a potential drug for the prevention and treatment of osteoporosis.

INTRODUCTION

Bone homeostasis refers to the process through which bone tissue, under its own regulation, keeps the dynamic equilibrium between bone creation and bone resorption.[1] Disruption of bone homeostasis can result from the dysregulation of the metabolic activity of osteoblasts and osteoclasts. Osteoclasts perform critical roles in the control of bone resorption in both healthy and pathological states.[2] Numerous osteolytic disorders can result from osteoclast hyperfunction.[3] As with postmenopausal osteoporosis, estrogen deprivation promotes transitory activation of osteoclasts, leading to bone loss, microstructural destruction, increased fragility, and increased fracture risk, which is frequently connected with life-threatening mortality and morbidity, and enormous economic consequences to people and society.[4]

Osteoclasts are the principal bone-resorbing cells in the current understanding.[5] Osteoclasts are multinucleated cells that have reached their final differentiation stage.[6] They are descended from monocytes in the hematopoietic stem cell lineage and are affected by various stimuli. These include macrophage colony stimulating factor (M-CSF) and receptor activators of nuclear factor-B (RANK) ligand (RANKL), both of which could be secreted by stromal cells and osteoblasts.[7–9] For RANKL and its receptor RANK, TNF receptor-associated factor 6 (TRAF6) functions as an adapter molecule.[10,11] The I kappa B kinases (IKKs) are responsible for the nuclear factor-κB (NF-κB)-induced production of proto-oncogene c-Fos (c-Fos), while the mitogen-activated kinases (MAPK) pathway is responsible for the activation of Jun proteins.[12] The activating protein-1 (AP-1) complex is formed when the proteins c-Fos and Jun bind to one another.[13] NFATc1, which plays an essential part in controlling the formation of osteoclasts, is mediated by AP-1 and NF-κB.[14,15] Furthermore, calcium oscillatory signaling regulates NFATc1, activating calcium-regulated neurophosphatases that facilitate NFATc1 dephosphorylation and encourage its entrance into the nucleus.[16] A series of genes, including the NFATc1 protein itself, can be activated by the transcription factor NFATc1 to produce an auto-amplifying loop.[17] Further induction of osteoclast-specific target gene expression consists of matrix metalloproteinase 9 (*Mmp9*), cathepsin K (*Ctsk*), acid phosphatase 5 (*Acp5*), v-ATPase V0 domain (*ATP6V0D2*) and dendritic cell-specific transmembrane protein (*Dc-stamp*).[18,19] Therefore, osteoclast transitional differentiation or its function can be successfully prevented by decreasing the RANKL-induced NFATc1 signaling pathway, having a therapeutic effect on osteoclast-associated skeletal disorders.

[1]Guangxi Key Laboratory of Regenerative Medicine, Orthopaedic Department, The First Affiliated Hospital of Guangxi Medical University, Nanning, Guangxi 530021, China
[2]Collaborative Innovation Centre of Regenerative Medicine and Medical BioResource Development and Application Co-constructed by the Province and Ministry, Life Sciences Institute, Guangxi Medical University, Nanning, Guangxi 530021, China
[3]School of Biomedical Sciences, University of Western Australia, Perth, WA 6009, Australia
[4]Shenzhen Institute of Advanced Technology, Chinese Academy of Sciences, Shenzhen 518000, China
[5]These authors contributed equally
[6]Lead contact
*Correspondence: liuqian@gxmu.edu.cn (Q.L.), zhaojinmin@126.com (J.Z.)
https://doi.org/10.1016/j.isci.2023.107760

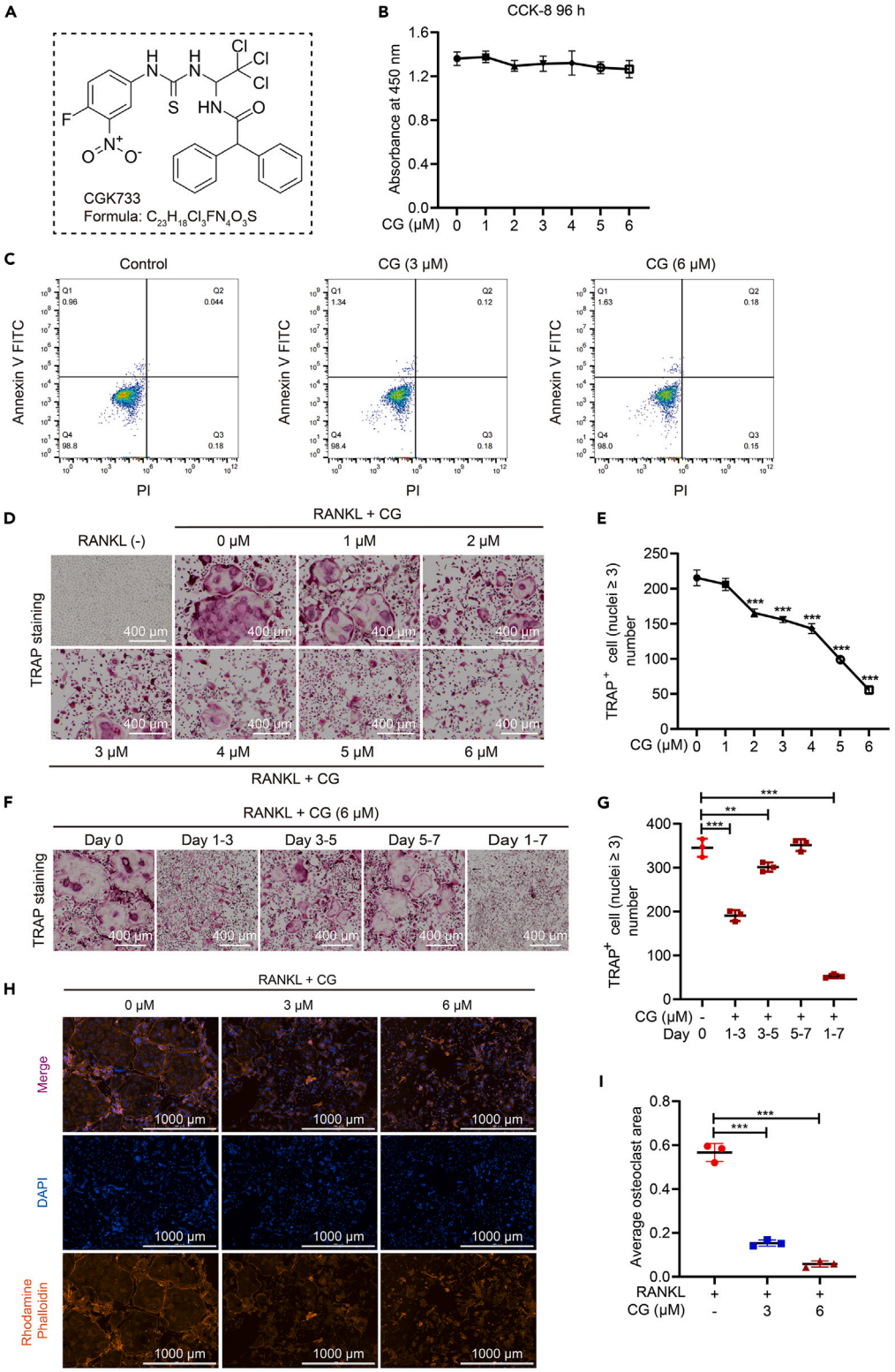

Figure 1. CG suppresses RANKL-induced osteoclastogenesis *in vitro*

(A) The chemical structure of CGK733 (CG).

(B) The cell viability of BMMs treated with CG was detected by CCK-8 assay (n = 3).

(C) Flow cytometry was applied to examine the apoptosis of BMMs treated with 3 μM and 6 μM CG for 48 h.

Figure 1. *Continued*

(D) TRAP staining images of BMMs cultured with or without RANKL in the presence of indicated concentrations of CG from 0 to 6 μM (scale bar = 400 μm).

(E) $TRAP^+$ osteoclasts were quantified in each well (nuclei ≥3).

(F) Stage representative images of $TRAP^+$ osteoclasts treated with CG (scale bar = 400 μm).

(G) Quantitative analysis of $TRAP^+$ osteoclasts (nuclei ≥3).

(H) Representative images of podosome belts in the presence or absence of CG (scale bar = 1000 μm).

(I) The podosome belt area was quantified by ImageJ software.

All data are presented as mean ± SD. Statistical significance was assessed via one-way ANOVA method. *$p < 0.05$, **$p < 0.01$, ***$p < 0.001$.

Currently, the principal treatment approaches for osteoporosis aim to constrain bone resorption and increase bone matrix production. Bisphosphonates, RANKL antibodies, and selective estrogen receptor modulators are examples of anti-bone resorption medications that prevent bone resorption.[20,21] Teriparatide is one example of a drug that helps build bone.[22] There is no denying that these medications work, but there are some unavoidable side effects, such as bisphosphonates, RANKL antibodies, which may lead to jaw bone death and atypical femur fractures,[23] selective estrogen receptor modulators, which may potentially increase the risk of endometrial and breast cancer with long-term use,[24] and teriparatide, which most commonly causes nausea, headaches, and dizziness.[25] Therefore, it is critical to investigate medications that can cure osteoporosis yet have fewer negative effects.

Ataxia telangiectasia mutated (ATM) is a serine-threonine protein kinase that belongs to the phosphatidylinositol 3-kinase-related kinase (PIKK) family. Capillary dilatation, ATM and Rad3-related (ATRs), and DNA-dependent protein kinases (DNAPKcs) are also in this group.[26] Early research found that the ATM/ATR inhibitor increased cellular sensitivity to radiotherapy by inhibiting DNA repair and cell cycle checkpoints in tumor cells.[27] ATM detects ionizing radiation and other DNA-damaging agents by activating multiple effectors and participating in various signaling pathways.[28] *In vivo* studies have shown that blocking the ATM-dependent NF-κB pathway increases chemotherapy sensitivity in acute lymphoblastic leukemia.[29] ATM deficiency also reduces neural stem cell proliferation via the oxidative stress-mediated p38 MAPK signaling pathway.[30] Current research indicates that this class of drugs can prevent osteoporosis,[31] but studies on the ATM/ATR inhibitor CG are lacking in this regard. Therefore, this study aimed to explore the anti-osteoporosis potential of CG.

RESULTS

CG reduces RANKL-induced osteoclast production *in vitro*

First, the toxicity of CG (Figure 1A) on BMMs was examined after 96 h; the CCK-8 assay revealed no cytotoxic impact on BMMs in the concentration range of 1–6 μM of CG (Figure 1B). Moreover, exposure of BMMs to 3 μM or 6 μM CG for 48 h did not affect apoptosis (Figure 1C). To find out if CG can prevent osteoclastogenesis, we cultured BMMs with different doses of CG (0, 1, 2, 3, 4, 5, and 6 μM) and stimulated with RANKL. CG reduced osteoclast formation dose-dependently within the safe range, with the highest impact at 6 μM (Figures 1D and 1E). To learn more about how CG affects the process of osteoclast development at various stages. The results showed that in BMMs stimulated with RANKL in culture for 7 days, CG had an inhibitory effect on the early and middle stages of the osteoclast formation process, more notably on the early stages of osteoclast differentiation (Figures 1F and 1G). Podosome belts are the symbol of mature osteoclasts, and osteoclasts attach to the bone matrix through the podosome belt. To examine how CG affects the podosome belt of the osteoclast cytoskeleton, we stained mature osteoclasts with rhodamine phalloidin and analyzed the resulting structural variation in the podosome belt (Figure 1H). Osteoclast function relies on the creation of podosome belts, and these podosome belts were visible in the Comparison group. In contrast, in the CG-treated group, a significant reduction in the area of the podosome belt was observed (Figure 1I). In addition, the effect of CG on osteoblast proliferation and differentiation was investigated in this study. The results showed that CG had no significant effect on the proliferation and differentiation of osteoblasts (Figure S1). According to the above results, CG inhibited RANKL-induced osteoclast development *in vitro* without having a discernible deleterious impact on the osteoclast.

CG inhibits the expression of NFATc1 and osteoclast-specific genes

The upregulation of related specific expression during RANKL stimulation of osteoclast formation boosts osteoclast maturation and bone resorption function. Thus, qPCR was performed to identify osteoclast-associated genes including *Dc-stamp*, *c-Fos*, *Mmp9, Ctsk, Acp5*, and *Nfatc1*. RANKL increased the expression of these genes in mature osteoclasts, while CG decreased it considerably (Figure 2A). Furthermore, the transcription factor NFATc1 is primarily responsible for controlling osteoclast formation. When this transcriptional mechanism is activated, it functions as a master switch to control downstream target genes such *as Ctsk* and *Atp6v0d2*. We analyzed the protein expression levels in BMMs following CG addition to learning more about the part that CG plays in the production of RANKL-induced osteoclasts. After 1, 3, and 5 days of RANKL stimulation of BMMs, CG administration for 3 days significantly suppressed NFATc1 protein expression in comparison to the control group, but no statistical significance was seen for 5 days. CTSK, ATP6V0D2, and c-Fos protein expression increased with time, whereas CG dramatically lowered CTSK, ATP6V0D2, and c-Fos protein expression, mostly at 3 and 5 days (Figure 2B). The findings showed that CG inhibited NFATc1 and c-Fos, which are needed for RANKL-mediated osteoclast formation. Meanwhile, CG blocked its downstream proteins such as CTSK and ATP6V0D2 (Figures 2C–2F). Taken together, CG prevents osteoclasts from generating and functioning via blocking the activation of NFATc1 and the expression of its downstream proteins.

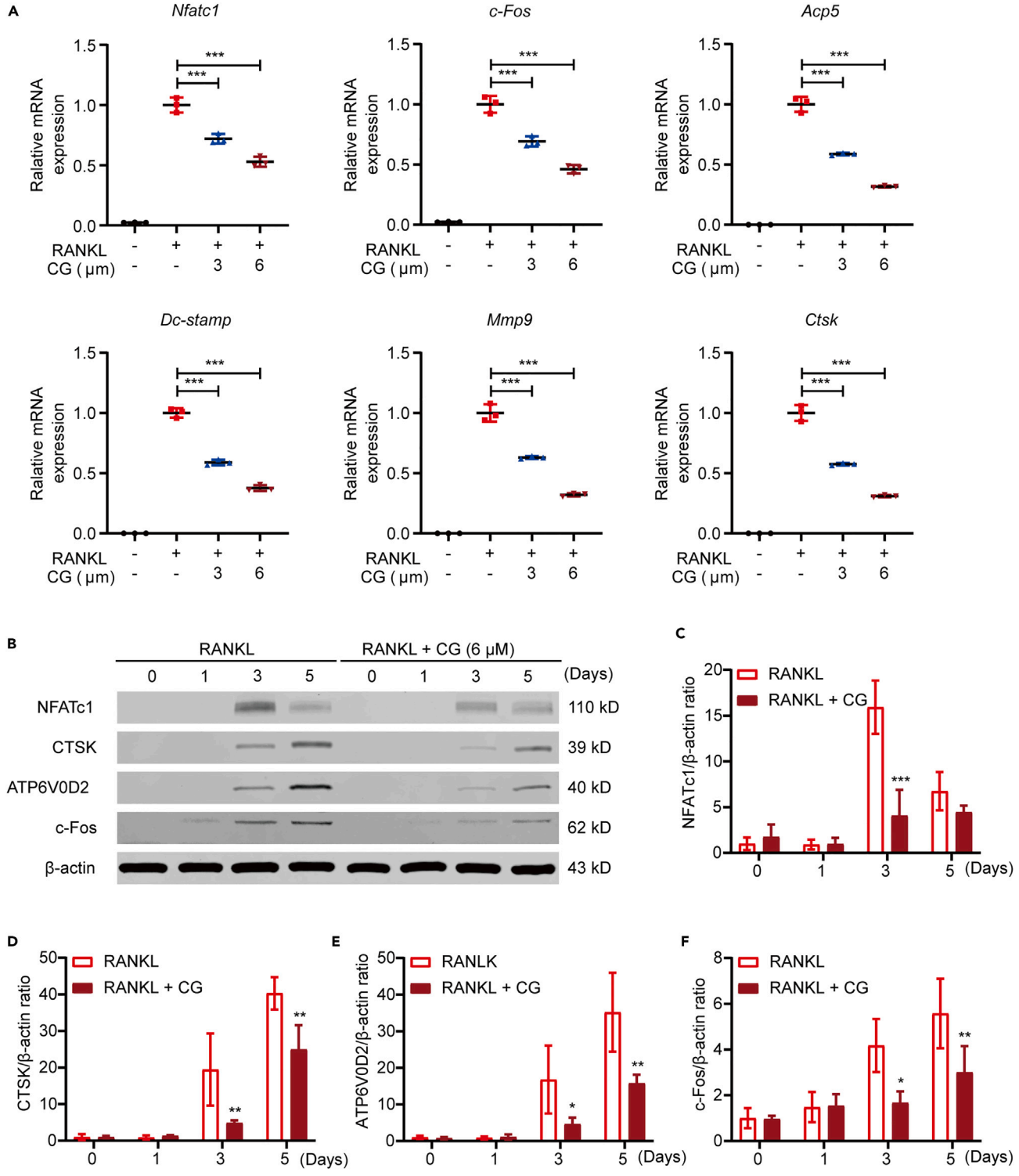

Figure 2. CG inhibits the expression of osteoclast-specific genes and RANKL-induced NFATc1

(A) qPCR was used to detect the expression levels of *Nfatc1*, *c-Fos*, *Acp5*, *Dc-stamp*, *Mmp9* and *Ctsk* relative to *β-actin* in BMMs stimulated with RANKL for 5 days in the presence of CG (n = 3). All data are presented as mean ± SD. Statistical significance was assessed via one-way ANOVA method.

(B) Representative Western blot images of the expression levels of NFATc1, CTSK, ATP6V0D2 and c-Fos. BMMs were cultured with or without CG treatment in the presence of RANKL for 1, 3, and 5 days, and the expression of related proteins was detected by western blot.

(C–F) Quantification of the ratios of band intensity of NFATc1, CTSK, ATP6V0D2, and c-Fos relative to β-actin (n = 3). All data are presented as mean ± SD. Statistical significance was assessed via two-way ANOVA method. *p < 0.05, **p < 0.01, ***p < 0.001.

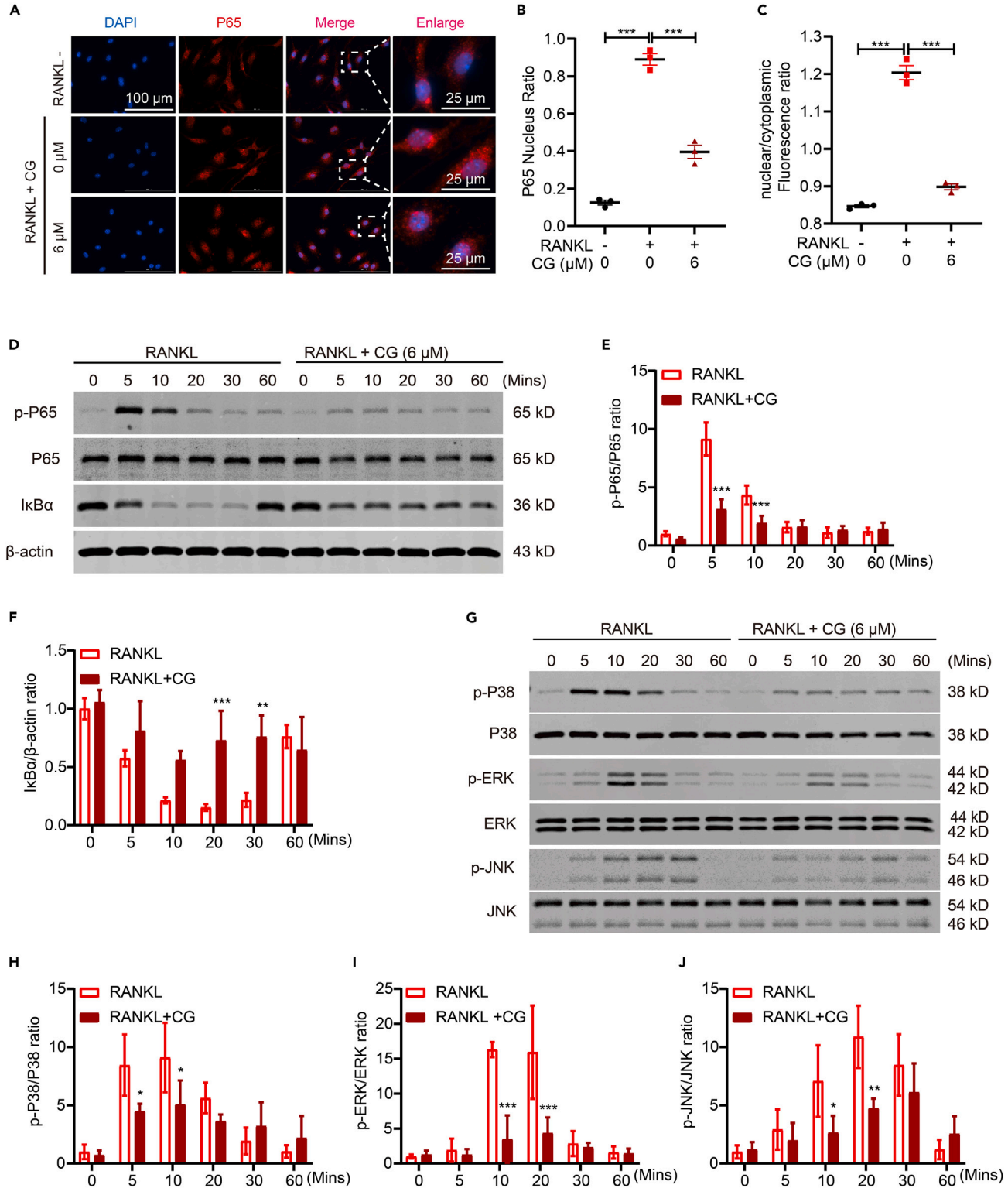

Figure 3. CG blocks RANKL-induced activation of the NF-κB/MAPK signaling pathway

(A) The representative immunofluorescence images of p65 nuclear translocation following RANKL stimulation for 30 min without or with CG (6 μM). (scale bar = 100 μm, the inset enlarged images scale bar = 25 μm).

(B and C) Quantification of nuclear translocation of P65 and nuclear/cytoplasmic Fluorescence ratio (n = 3). All data are presented as mean ± SD. Statistical significance was assessed via one-way ANOVA method.

Figure 3. *Continued*

(D) Representative western blot images of the effects of CG on P65 phosphorylation and IκBα degradation induced by RANKL. BMMs starved for 3 h with or without CG pretreatment were stimulated with RANKL (50 ng/mL) at series time points (0, 5, 10, 20, 30, 60 min). The expression of total and phosphorylated proteins was detected by western blot.

(E and F) Quantification of the ratios of band intensity of p-P65 relative to P65 and IκBα relative to β-actin. (n = 3).

(G) Representative Western blot images of the effects of CG on MAPK pathway. The effect of CG on RANKL-induced activation of P38, ERK, and JNK was detected by Western blot.

(H–J) The ratios of phosphorylated and non-phosphorylated forms of P38, ERK and JNK were quantified (n = 3).

All data are presented as mean ± SD. Statistical significance was assessed via two-way ANOVA method. *p < 0.05, **p < 0.01, ***p < 0.001.

CG blocks the NF-κB/MAPK signaling pathways

To further understand the mechanism of CG-mediated suppression of NFATc1 activation, we looked into NFATc1 upstream signaling networks, such as NF-κB and MAPK. Immunofluorescence staining revealed a substantial decrease in P65 nuclear translocation after CG treatment compared with the control group (Figures 3A–3C). Following that, we investigated whether CG affected NF-κB/MAPK signaling pathway using Western blotting. The experimental results revealed that CG reduced P65 phosphorylation at 5 and 10 min and inhibitor of nuclear factor kappa B alpha (IκBα) degradation at 20 and 30 min (Figures 3D–3F). The findings demonstrated that CG effectively suppressed P65 nuclear translocation. Additionally, western blotting showed that CG made ERK, P38, and JNK less phosphorylated (Figure 3G). P38 phosphorylation was suppressed by CG at 5 and 10 min, whereas ERK and JNK phosphorylation was considerably decreased at 10 and 20 min (Figures 3H–3J). In conclusion, CG inhibits osteoclast growth by lowering inhibition of osteoclast formation by dampening stimulation of the NF-κB/MAPK signaling pathway.

CG suppresses osteoclast bone resorption and the oscillation of intracellular Ca^{2+}

The next step, to see if CG inhibits osteoclast activity in bovine bone chips, hence reducing bone resorption. RANKL matured the BMMs into osteoclasts, which were then cultured by adding 0, 3 or 6 μM CG. Using scanning electron microscopy, bone chips were observed (Figure 4A), and we used ImageJ to measure the bone resorption area. The data revealed that there was a dose-dependent inhibition of absorption function by CG (Figures 4B and 4C). Given that calcium signaling can influence various life activity systems such as osteoclast motility, function, and apoptosis. We analyzed the impact of CG on RANKL-induced intracellular calcium oscillations to determine the molecular mechanism by which CG inhibits osteoclast formation and activity. Calcium signaling is triggered in response to RANKL stimulation, resulting in calcium oscillations that induce NFATc1 nuclear translocation and self-amplification. RANKL stimulation increased Ca^{2+} oscillations compared to the control group, while CG therapy significantly reduced RANKL-induced Ca^{2+} oscillations (Figures 4D and 4E).

CG prevents estrogen deficiency-induced osteoporosis

Based on the results of *in vitro* testing, we explored further the potential therapeutic effects of CG. This study used an OVX mouse model to simulate systemic osteoporosis. After surgery, mice were given intraperitoneal injections of E_2 (100 ng/kg), CG (3 or 6 mg/kg), or saline every other day for 6 weeks (Figure 5A). Throughout the pharmacological treatment period, the mice gained weight steadily with no notable differences between groups (Figure 5B). Neither infections nor fatalities were noted in the mice while they were receiving the medication. H&E staining of the heart, liver, and kidney revealed that CG had no effect on the cell morphology (Figure S2). Additionally, serological index analysis demonstrated that CG successfully decreased the expression of CTX-1, an osteoclast-specific marker (Figure 5C). Bone loss caused by OVX was reduced by E_2 and CG, according to micro-CT assay (Figure 5D). The distal femur was analyzed by micro-CT for BV/TV, Tb.Sp, Tb.N, and Tb.Th, all of which are bone-related features. When compared with the control group, CG treatment caused significantly less bone loss (Figures 5E–5H). H&E staining of mice femoral sections provided additional evidence of the improvement in bone volume following CG therapy. The H&E staining and TRAP staining findings revealed that the CG-treated group had considerably more bone trabecular volume and fewer TRAP-positive osteoclasts than the OVX-treated group (Figures 6A, 6B, 6D, and 6E). Meanwhile, immunohistochemical staining demonstrated that CG therapy decreased CTSK-positive cell area (Figures 6C and 6F). As expected, CG protected against estrogen deficiency-induced bone loss.

DISCUSSION

Osteoporosis is a systemic skeletal disorder characterized by decreasing bone mass, degradation of the bone microarchitecture, increased bone fragility, and an elevated risk of fracture.[32] Although it can happen at any age, it is more common in postmenopausal women and older males. Excessive number and hyperfunction of osteoclasts are the primary causes of various osteolytic disorders, such as osteoporosis and periprosthetic joint replacement.[33] The current drugs for osteoporosis are effective but have many side effects and are less effective in tumor-related bone loss. The main clinical application of CG is tumor sensitization, however, its potential in preventing bone loss is unknown.

This work shows how CG inhibits NF-κB/MAPK signaling pathway and Ca^{2+} oscillations, which prevents NFATc1 activation, to impact osteoclast development and function *in vitro*. The present research also showed that CG worked very well in the OVX mouse model of bone loss caused by a lack of estrogen.

RANKL signaling and osteoclast development are closely connected processes. Through its receptor RANK, RANKL starts a signaling cascade.[34] Next, TRAF6 and adhesion molecules engage the NF-κB and MAPK signaling pathways, which in turn activate transcriptional

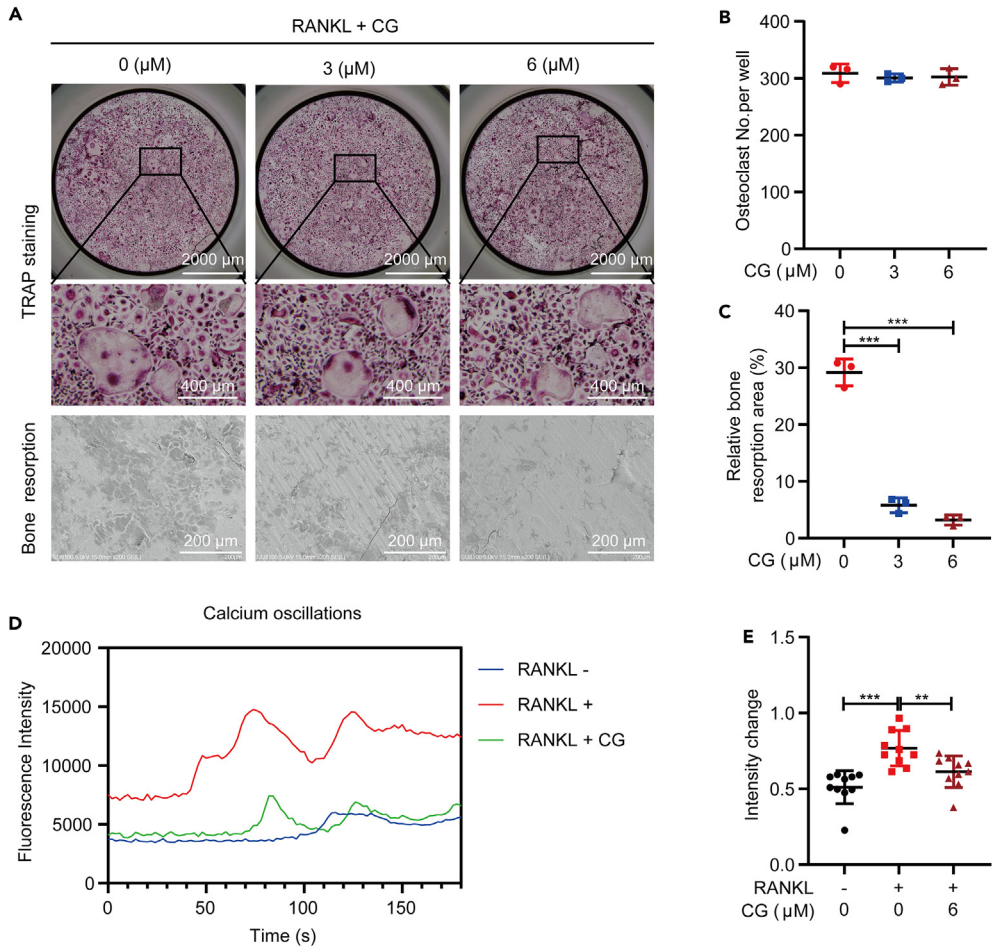

Figure 4. CG attenuates Ca^{2+} oscillations and bone resorption activity of osteoclasts *in vitro*

(A) Representative images of bone resorption areas formed by osteoclasts that were treated with CG were obtained by scanning electron microscopy (scale bar = 200 μm) and representative images of TRAP-stained cells (scale bar = 2000 μm, the inset enlarged images scale bar = 400 μm).

(B and C) The area of bone resorption pits and TRAP-positive cells per well was quantified using ImageJ software (n = 3).

(D) Line chart of Ca^{2+} oscillatory fluorescence intensity from negative control, positive control, and CG (6 μM) treated groups.

(E) Quantitative analysis of changes in Ca^{2+} oscillation intensity in each group (n = 10 cells per group). The values of intensity change were calculated by the maximum peak intensity minus the minimum intensity and then comparing it to the average value.

All data are presented as mean ± SD. Statistical significance was assessed via one-way ANOVA method. *p < *0.05*, **p < *0.01*, ***p < *0.001*.

regulators and cause the development of bone breakdown processes. NF-κB activators control osteoclast development, and bone resorption, which are essential for preserving calcium homeostasis.[35,36] It has been shown that when NF-κB subunits p50 and p52 are deleted at the same time in mice, osteoclast formation is limited, which leads to osteosclerosis.[37] The macromolecular IκB kinase complex (IKK) phosphorylates IκBα protein in the conventional pathway of NF-κB activation, followed by fast ubiquitination and subsequent destruction of IκBα protein via the ubiquitin-mediated proteasomal degradation pathway. When IκBα is degraded, the NF-κB protein is able to translocate from the cytoplasm to the nucleus and attach to its cognate DNA binding site, controlling transcription of downstream target genes.[38,39] Overaction of NF-κB in osteoclasts is associated with a set of osteolytic diseases.[40,41] Here, we found that CG blocks NF-κB pathway activation by preventing P65 nuclear translocation, P65 phosphorylation, and IkBα degradation. TRAF6 recruits RANKL and RANK binding to activate the MAPK pathway, which includes ERK, JNK, and p38.[42] When it comes to osteoclast differentiation and survival, ERK signaling is crucial.[43,44] One study found that cells from JNK1-deficient bone marrow did not differentiate into osteoclasts, indicating that JNK1 activation plays an essential regulatory function in osteoclast formation.[45] p38 is also critical in the formation of osteoclasts.[46] Our further research revealed that CG could also decrease the phosphorylation of ERK, JNK, and P38, which has an impact on how the MAPK signaling pathway is activated by RANKL.

NFATc1 is a dominant transcription factor in osteoclastogenesis.[47–49] There is a large body of evidence demonstrating that embryonic stem cells lacking NFATc1 fail to develop into osteoclasts. furthermore, NFATc1 knockout mice have severe osteosclerosis.[50–52] It regulates various osteoclast-specific genes, including *Acp5*, *Mmp9*, *Ctsk*, and *Dc-stamp*, through binding to MITF and c-Fos, which is critical for the formation of osteoclasts. c-Fos is an essential part of the AP-1 activator protein, which functions as a transcription factor.[17,53] c-Fos is

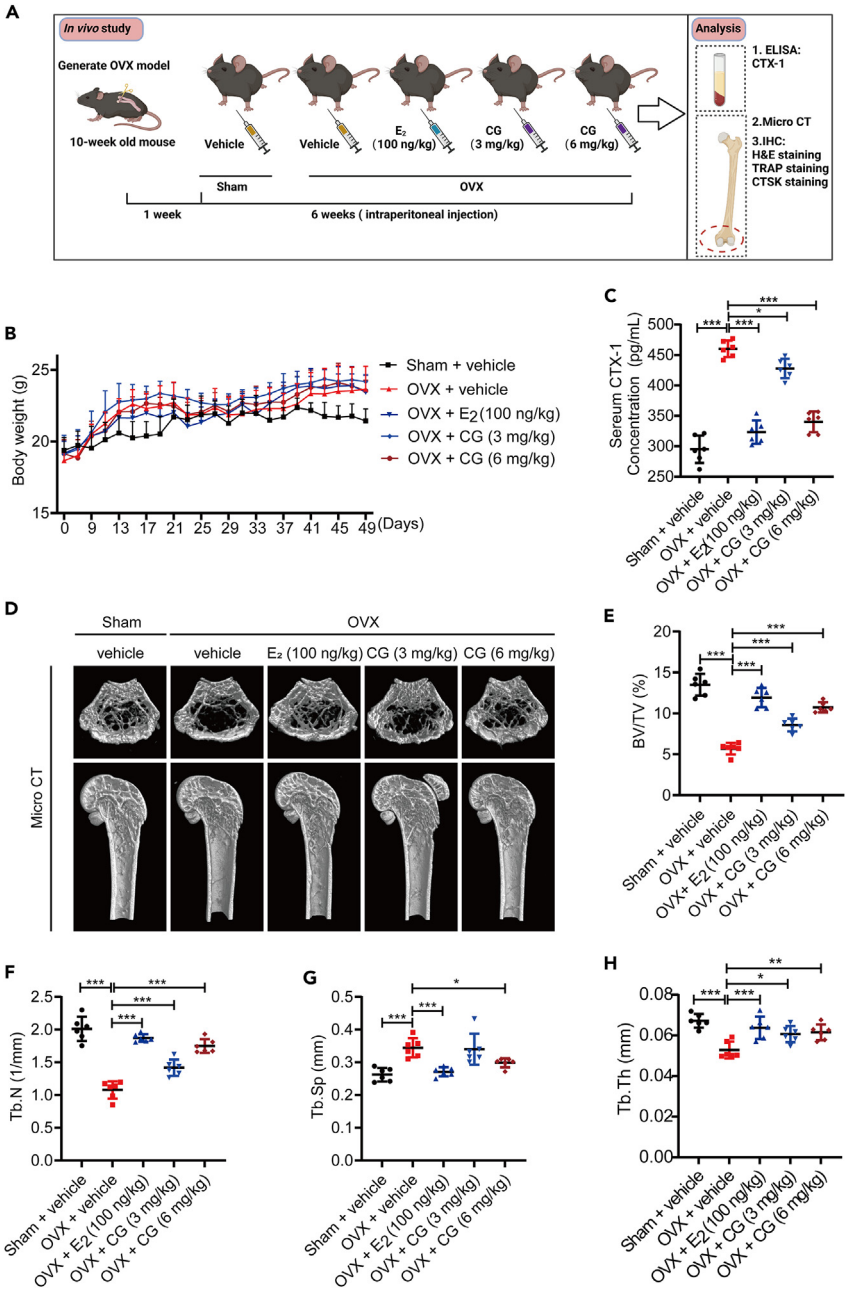

Figure 5. CG treatment prevents bone loss induced by ovariectomized *in vivo*

(A) Diagram of the process and grouping of animal experiments was created by https://www.biorender.com/. ELISA, enzyme-linked immunosorbent assay; IHC, immunohistochemistry.

(B) Weight curve of mice following OVX surgery at various time periods (n = 6 mice per group).

(C) CTX-1 levels in serum were measured using an ELISA kit (n = 6 mice per group).

(D) Representative of Micro CT images showed that the bone loss was prevented by CG administration (n = 6 mice per group).

(E–H) Quantitative analysis of parameters relating to bone microstructure, including volume/tissue volume (BV/TV), the trabecular number (Tb. N), the trabecular separation (Tb. Sp), and the trabecular thickness (Tb. Th) (n = 6 mice per group).

All data are presented as mean ± SD. Statistical significance was assessed via one-way ANOVA method. *p < *0.05*, **p < *0.01*, ***p < *0.001*.

considered a direct regulator of NFATc1 since it is recruited to the NFATc1 promoter during early osteoclast formation. Mice deficient c-Fos developed osteosclerosis.[54] In this research, the transcriptional activity of NFATc1 and c-Fos as well as the expression of their downstream transcription factors were both considerably repressed by CG. Specifically, NFATc1 and its downstream proteins ATP6V0D2, MMP-9, and

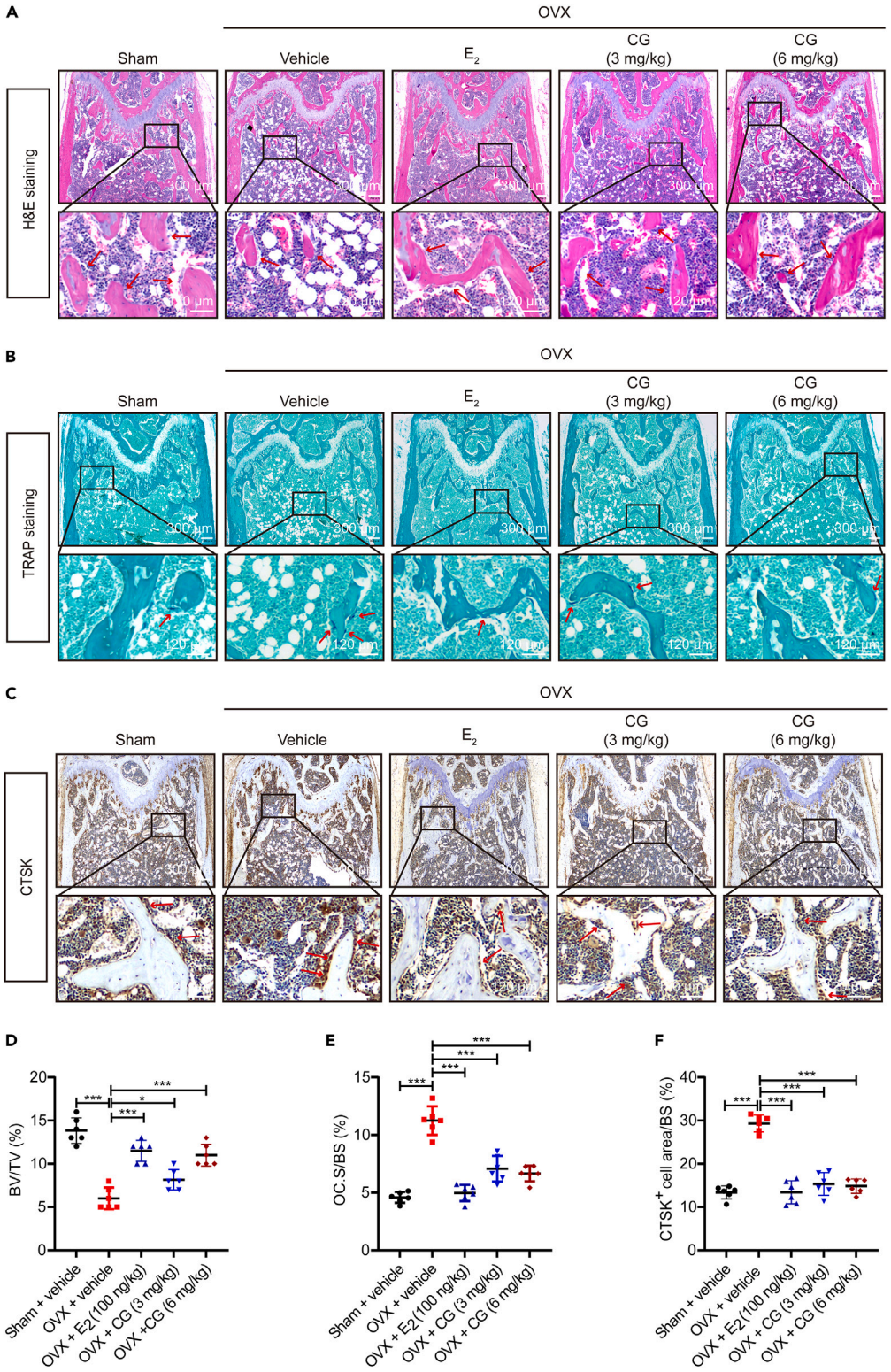

Figure 6. CG ameliorates osteoclast activity in a mouse model of osteoporosis induced by ovariectomized

(A) Representative images of histological analysis of the left femur stained with H&E.

(B) Representative images of histological analysis of the left femur stained with TRAP.

(C) CTSK-positive cells were marked as brownish-yellow (scale bar = 300 μm, the inset enlarged images scale bar = 120 μm).

Figure 6. *Continued*

(D) BV/TV was quantitatively analyzed in tissue sections (n = 6 mice per group).

(E) TRAP-positive osteoclast surface per trabecular surface (OC. S/BS) was quantitatively analyzed (n = 6 mice per group).

(F) The level of CTSK was quantitatively measured in the left femur (n = 6 mice per group).

All data are presented as mean ± SD. Statistical significance was assessed via one-way ANOVA method. *p < *0.05*, **p < *0.01*, ***p < *0.001*.

CTSK were significantly elevated in response to RANKL activation, whereas CG significantly curbed the expression of these proteins. This could be a result of CG disrupting the NF-B/MAPK signaling pathway.

Calcium (Ca^{2+}) is vital for the regulation of osteoclast development and function. Ca^{2+} oscillations are a bone resorption and osteoclastogenesis phenomenon caused by RANKL via calcium-regulated neurophosphatase.[55,56] RANKL activates NFATc1 gene transcription and protein expression by inducing sustained calcium oscillations in BMMs, which in turn activates ATP6V0D2, MMP-9, and CTSK, thereby promoting acid secretion and organic matter degradation by osteoclasts and accelerating bone loss.[57] We discovered that RANKL-induced Ca^{2+} oscillations were reduced by CG treatment, implying that CG affects the auto-amplification of NFATc1, at least in part by inhibiting Ca^{2+} oscillations, and thus inhibits the bone resorption function of osteoclasts. Considering the intimate relationship between osteoblasts and osteoclasts as well as the crucial function that osteoblasts also perform in bone remodeling. The effects of CG on the generation of osteoblasts were also studied by ALP, and the results showed that CG did not influence osteoblasts.

Finally, we used the OVX mouse model to examine whether CG has *in vivo* a healing effect on osteoporosis. Micro-CT scans revealed a severe bone loss in mice after OVX surgery, which CG reversed in a dose-dependent manner, similar to the effect of E_2. Specifically, the OVX group had the lowest TV/BV, and this index increased significantly with the use of CG; Tb.N and Tb.Th exhibited a similar pattern. Conversely, the OVX group had the highest Tb.Sp, and CG significantly decreased this index. Consistent with the results of the Micro-CT scan, CG significantly decreased osteoclasts *in vivo* and increased bone mass, as evidenced by the TRAP and H&E staining results of bone tissue. Immunohistochemical analysis of bone tissue revealed that CG significantly inhibited CTSK expression in the OVX mouse model. Furthermore, CG had no significant toxic effects on the heart, liver, or kidneys of mice.

In conclusion, our findings show that CG inhibited NFATc1 through the RANKL-induced Ca^{2+} oscillations signaling and NF-κB/MAPK pathway, which suppressed osteoclast formation and its bone resorption function (Figure 7). CG was also found to improve bone loss in OVX mice. Therefore, CG may be an efficient treatment option for the treatment of osteoclast-mediated osteolytic diseases like osteoporosis.

Limitations of the study

Our research is mainly conducted *in vitro* and *in vivo*. *In vitro*, we found that CG inhibited osteoclast differentiation and its bone resorption function by inhibiting RANKL-mediated Ca^{2+} oscillations and the NF-κB/MAPK signaling pathway. And further sequencing is needed to search for a more specific molecular mechanism by which CG regulates osteoclast differentiation and function. *In vivo*, we constructed an

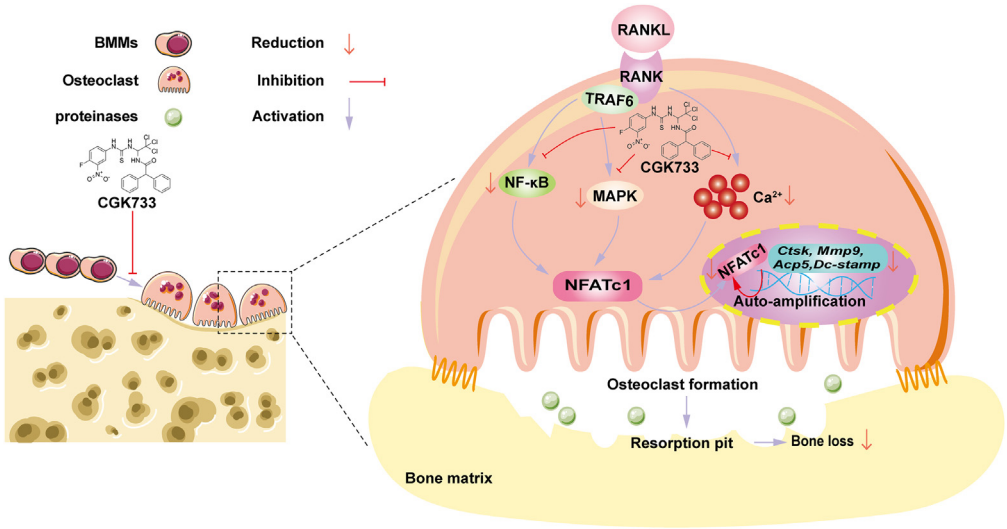

Figure 7. A proposed scheme depicting the inhibition of CG on RANKL-induced NFATc1 activation during osteoclast differentiation

Our findings demonstrate that CG suppresses NFATc1 activation and downregulates osteoclast-specific genes such as *Mmp9, Dc-stamp, Ctsk, and Acp5* via inhibiting the calcium signaling pathway and the RANKL-induced NF-B/MAPK signaling pathway. NFATc1, nuclear factor of activated T cells 1; Mmp9, matrix metallopeptidase 9; Ctsk, cathepsin K; Dc-stamp, dendritic cell-specific transmembrane protein; Acp5, tartrate-resistant acid phosphatase; RANKL, receptor activator of nuclear factor-κB (NF-κB) ligand; NF-κB, nuclear factor-κB; MAPKs, mitogen-activated protein kinases.

OVX mouse model to verify that CG ameliorates bone loss in estrogen deficiency, and it may be necessary to verify the role of CG in ameliorating bone loss in a different model of osteoporosis.

STAR★METHODS

Detailed methods are provided in the online version of this paper and include the following:

- KEY RESOURCES TABLE
- RESOURCE AVAILABILITY
  - Lead contact
  - Materials availability
  - Data and code availability
- EXPERIMENTAL MODEL AND STUDY PARTICIPANT DETAILS
  - Animals
  - Bone marrow macrophages extraction
  - OVX model
- METHOD DETAILS
  - Materials and reagents
  - Animal ethics
  - Cell culture
  - Cytotoxicity assay
  - Osteoclastogenesis assay
  - Podosome belt staining
  - Immunofluorescence staining
  - Bone resorption assay
  - Intracellular calcium (Ca^{2+}) oscillation assay
  - Relative quantitative PCR (qPCR)
  - Western blot assay
  - Osteoporotic ovariectomized (OVX) model mice
  - Micro-computed tomography (Micro-CT)
  - Histological assessment
  - Differentiation of osteoblast precursor
  - ELISA assay
- QUANTIFICATION AND STATISTICAL ANALYSIS

SUPPLEMENTAL INFORMATION

Supplemental information can be found online at https://doi.org/10.1016/j.isci.2023.107760.

ACKNOWLEDGMENTS

This research was supported by the National Natural Science Foundation of China (Grant No. 81960405), the Guangxi Science and Technology Base and Talent Special Project (Grant No. GuikeAD19254003), and the Guangxi Natural Science Foundation (2021GXNSFAA196039). It is also partly supported by the open research fund from the Collaborative Innovation Center of Regenerative Medicine and Medical Bioresource Development and Application Co-constructed by the Province and Ministry, and the Training Program for One Thousand Young and Middle-aged Backbone Teachers in Guangxi Colleges and Universities.

AUTHOR CONTRIBUTIONS

M.X.: Writing–first draft, visualization. D.S.: Data curation, writing – review and editing, validation. X.X.: Formal analysis. Y.Q., J.H.: Methodology. C.W.: Experimental assistance. J.C.: Investigation. Y.S.: Software support. J.X.: Design, writing – review and editing. J.Z.: Project administration, Funding acquisition. Q.L.: Supervision, Writing – review and editing, Funding acquisition.

DECLARATION OF INTERESTS

The authors declare that there are no conflicts of interest.

INCLUSION AND DIVERSITY

We support inclusive, diverse, and equitable conduct of research.

Received: May 11, 2023
Revised: August 20, 2023
Accepted: August 25, 2023
Published: August 29, 2023

REFERENCES

1. Kim, H.J., Seong, H.S., Choi, Y., Heo, S.C., and Kim, Y.D. (2020). Letrozole Suppresses the Fusion of Osteoclast Precursors through Inhibition of p38-Mediated DC-STAMP Pathway. Int. J. Mol. Sci. *21*, 8396.
2. Zhang, Z., Wen, H., Yang, X., Zhang, K., He, B., Zhang, X., and Kong, L. (2019). Stimuli and Relevant Signaling Cascades for NFATc1 in Bone Cell Homeostasis: Friend or Foe? Curr. Stem Cell Res. Ther. *14*, 239–243.
3. Zhang, J., Yang, Z., and Dong, J. (2016). P62: An emerging oncotarget for osteolytic metastasis. J. Bone Oncol. *5*, 30–37.
4. Chen, K., Qiu, P., Yuan, Y., Zheng, L., He, J., Wang, C., Guo, Q., Kenny, J., Liu, Q., Zhao, J., et al. (2019). Pseurotin A Inhibits Osteoclastogenesis and Prevents Ovariectomized-Induced Bone Loss by Suppressing Reactive Oxygen Species. Theranostics *9*, 1634–1650.
5. Wu, M., Chen, W., Lu, Y., Zhu, G., Hao, L., and Li, Y.P. (2017). Gα13 negatively controls osteoclastogenesis through inhibition of the Akt-GSK3β-NFATc1 signalling pathway. Nat. Commun. *8*, 13700.
6. Lian, J.B., Stein, G.S., van Wijnen, A.J., Stein, J.L., Hassan, M.Q., Gaur, T., and Zhang, Y. (2012). MicroRNA control of bone formation and homeostasis. Nat. Rev. Endocrinol. *8*, 212–227.
7. Zhan, Y., Liang, J., Tian, K., Che, Z., Wang, Z., Yang, X., Su, Y., Lin, X., Song, F., Zhao, J., et al. (2019). Vindoline Inhibits RANKL-Induced Osteoclastogenesis and Prevents Ovariectomy-Induced Bone Loss in Mice. Front. Pharmacol. *10*, 1587.
8. Kim, J.Y., Baek, J.M., Ahn, S.J., Cheon, Y.H., Park, S.H., Yang, M., Choi, M.K., and Oh, J. (2016). Ethanolic extract of Schizonepeta tenuifolia attenuates osteoclast formation and activation in vitro and protects against lipopolysaccharide-induced bone loss in vivo. BMC Complement. Altern. Med. *16*, 301.
9. Matsuike, R., Nakai, K., Tanaka, H., Ozaki, M., Kanda, M., Nagasaki, M., Shibata, C., Mayahara, K., Tanabe, N., Koshi, R., et al. (2019). Continuous Compressive Force Induces Differentiation of Osteoclasts with High Levels of Inorganic Dissolution. Med. Sci. Monit. *25*, 3902–3909.
10. Lee, K., Chung, Y.H., Ahn, H., Kim, H., Rho, J., and Jeong, D. (2016). Selective Regulation of MAPK Signaling Mediates RANKL-dependent Osteoclast Differentiation. Int. J. Biol. Sci. *12*, 235–245.
11. Wang, T., Liu, Q., Zhou, L., Yuan, J.B., Lin, X., Zeng, R., Liang, X., Zhao, J., and Xu, J. (2015). Andrographolide Inhibits Ovariectomy-Induced Bone Loss via the Suppression of RANKL Signaling Pathways. Int. J. Mol. Sci. *16*, 27470–27481.
12. Ma, M., Fan, A.Y., Liu, Z., Yang, L.Q., Huang, J.M., Pang, Z.Y., and Yin, F. (2022). Baohuoside I Inhibits Osteoclastogenesis and Protects Against Ovariectomy-Induced Bone Loss. Front. Pharmacol. *13*, 874952.
13. Malhi, S.M., Jawed, H., Hanif, F., Ashraf, N., Zubair, F., Siddiqui, B.S., Begum, S., Kabir, N., and Simjee, S.U. (2014). Modulation of c-Fos and BDNF protein expression in pentylenetetrazole-kindled mice following the treatment with novel antiepileptic compound HHL-6. BioMed Res. Int. *2014*, 876712.
14. Phromnoi, K., Suttajit, M., Saenjum, C., and Limtrakul Dejkriengkraikul, P. (2021). Inhibitory Effect of a Rosmarinic Acid-Enriched Fraction Prepared from Nga-Mon (Perilla frutescens) Seed Meal on Osteoclastogenesis through the RANK Signaling Pathway. Antioxidants *10*, 307.
15. Bak, S.U., Kim, S., Hwang, H.J., Yun, J.A., Kim, W.S., Won, M.H., Kim, J.Y., Ha, K.S., Kwon, Y.G., and Kim, Y.M. (2017). Heme oxygenase-1 (HO-1)/carbon monoxide (CO) axis suppresses RANKL-induced osteoclastic differentiation by inhibiting redox-sensitive NF-κB activation. BMB Rep. *50*, 103–108.
16. Liu, Y., Wang, C., Wang, G., Sun, Y., Deng, Z., Chen, L., Chen, K., Tickner, J., Kenny, J., Song, D., et al. (2019). Loureirin B suppresses RANKL-induced osteoclastogenesis and ovariectomized osteoporosis via attenuating NFATc1 and ROS activities. Theranostics *9*, 4648–4662.
17. Chen, X., Wang, C., Qiu, H., Yuan, Y., Chen, K., Cao, Z., Xiang Tan, R., Tickner, J., Xu, J., and Zou, J. (2019). Asperpyrone A attenuates RANKL-induced osteoclast formation through inhibiting NFATc1, Ca(2+) signalling and oxidative stress. J. Cell Mol. Med. *23*, 8269–8279.
18. Kanemoto, S., Kobayashi, Y., Yamashita, T., Miyamoto, T., Cui, M., Asada, R., Cui, X., Hino, K., Kaneko, M., Takai, T., et al. (2015). Luman is involved in osteoclastogenesis through the regulation of DC-STAMP expression, stability and localization. J. Cell Sci. *128*, 4353–4365.
19. Wang, X., Chen, X., Zhang, Z., Chen, J., Ge, Z., Huang, S., Wei, H., and Li, D. (2022). Asperuloside Prevents Peri-Implantitis via Suppression of NF-κB and ERK1/2 on Rats. Pharmaceuticals *15*, 1027.
20. Al Mamun, M.A., Asim, M.M.H., Sahin, M.A.Z., and Al-Bari, M.A.A. (2020). Flavonoids compounds from Tridax procumbens inhibit osteoclast differentiation by down-regulating c-Fos activation. J. Cell Mol. Med. *24*, 2542–2551.
21. Siegenthaler, B., Ghayor, C., Gjoksi-Cosandey, B., Ruangsawasdi, N., and Weber, F.E. (2018). The Bromodomain Inhibitor N-Methyl pyrrolidone Prevents Osteoporosis and BMP-Triggered Sclerostin Expression in Osteocytes. Int. J. Mol. Sci. *19*, 3332.
22. Bodenner, D., Redman, C., and Riggs, A. (2007). Teriparatide in the management of osteoporosis. Clin. Interv. Aging *2*, 499–507.
23. Wissing, M.D. (2015). Chemotherapy- and irradiation-induced bone loss in adults with solid tumors. Curr. Osteoporos. Rep. *13*, 140–145.
24. Cavalli, L., and Brandi, M.L. (2012). Targeted approaches in the treatment of osteoporosis: differential mechanism of action of denosumab and clinical utility. Ther. Clin. Risk Manag. *8*, 253–266.
25. Enishi, T., Uemura, H., Katoh, S., Inatsugi, M., Minato, S., Inatsugi, K., Inatsugi, M., Sato, N., and Siryo, K. (2015). Transient severe hypotension with once-weekly subcutaneous injection of teriparatide in osteoporotic patient: a case report and insight for the drug interaction between hypotensive agents and teriparatide. J. Med. Invest. *62*, 93–96.
26. Shiloh, Y., and Ziv, Y. (2012). The ATM protein: the importance of being active. J. Cell Biol. *198*, 273–275.
27. Mei, L., Zhang, J., He, K., and Zhang, J. (2019). Ataxia telangiectasia and Rad3-related inhibitors and cancer therapy: where we stand. J. Hematol. Oncol. *12*, 43.
28. Carr, M.I., Roderick, J.E., Gannon, H.S., Kelliher, M.A., and Jones, S.N. (2016). Mdm2 Phosphorylation Regulates Its Stability and Has Contrasting Effects on Oncogene and Radiation-Induced Tumorigenesis. Cell Rep. *16*, 2618–2629.
29. Chen, Y.L., Tang, C., Zhang, M.Y., Huang, W.L., Xu, Y., Sun, H.Y., Yang, F., Song, L.L., Wang, H., Mu, L.L., et al. (2019). Blocking ATM-dependent NF-κB pathway overcomes niche protection and improves chemotherapy response in acute lymphoblastic leukemia. Leukemia *33*, 2365–2378.
30. Kim, J., and Wong, P.K.Y. (2009). Loss of ATM impairs proliferation of neural stem cells through oxidative stress-mediated p38 MAPK signaling. Stem Cell. *27*, 1987–1998.
31. Yang, S., Song, D., Wang, Z., Su, Y., Chen, J., Xian, Y., Huang, J., Li, J., Xu, J., Zhao, J., and Liu, Q. (2022). AKT/GSK3β/NFATc1 and ROS signal axes are involved in AZD1390-mediated inhibitory effects on osteoclast and OVX-induced osteoporosis. Int. Immunopharmacol. *113*, 109370.
32. Peng, X., Wu, X., Zhang, J., Zhang, G., Li, G., and Pan, X. (2018). The role of CKIP-1 in osteoporosis development and treatment. Bone Joint Res. *7*, 173–178.
33. Wang, L., Chen, K., He, J., Kenny, J., Yuan, Y., Chen, J., Liu, Q., Tan, R., Zhao, J., and Xu, J. (2019). Cytochalasin Z11 inhibits RANKL-induced osteoclastogenesis via suppressing NFATc1 activation. RSC Adv. *9*, 38438–38446.
34. Lee, J., Ahn, S.H., Chen, Z., Kang, S., Choi, D.K., Moon, C., Min, S.H., Park, B.J., and Lee, T.H. (2020). N-[2-(4-Acetyl-1-Piperazinyl) Phenyl]-2-(3-Methylphenoxy)Acetamide (NAPMA) Inhibits Osteoclast Differentiation and Protects against Ovariectomy-Induced Osteoporosis. Molecules *25*, 4855.
35. Tan, P., Guan, H., Xie, L., Mi, B., Fang, Z., Li, J., and Li, F. (2015). FOXO1 inhibits osteoclastogenesis partially by antagnozing MYC. Sci. Rep. *5*, 16835.
36. Chen, X., Zhi, X., Pan, P., Cui, J., Cao, L., Weng, W., Zhou, Q., Wang, L., Zhai, X., Zhao, Q., et al. (2017). Matrine prevents bone loss in ovariectomized mice by inhibiting RANKL-induced osteoclastogenesis. FASEB J. *31*, 4855–4865.

37. Yan, L., Lu, L., Hu, F., Shetti, D., and Wei, K. (2019). Piceatannol attenuates RANKL-induced osteoclast differentiation and bone resorption by suppressing MAPK, NF-κB and AKT signalling pathways and promotes Caspase3-mediated apoptosis of mature osteoclasts. R. Soc. Open Sci. *6*, 190360.
38. Liu, M., Zhang, S.S., Liu, D.N., Yang, Y.L., Wang, Y.H., and Du, G.H. (2021). Chrysomycin A Attenuates Neuroinflammation by Down-Regulating NLRP3/Cleaved Caspase-1 Signaling Pathway in LPS-Stimulated Mice and BV2 Cells. Int. J. Mol. Sci. *22*, 6799.
39. Tsuchida, S., Satoh, M., Takiwaki, M., and Nomura, F. (2017). Ubiquitination in Periodontal Disease: A Review. Int. J. Mol. Sci. *18*, 1476.
40. Xu, J., Wu, H.F., Ang, E.S.M., Yip, K., Woloszyn, M., Zheng, M.H., and Tan, R.X. (2009). NF-kappaB modulators in osteolytic bone diseases. Cytokine Growth Factor Rev. *20*, 7–17.
41. Liu, Q., Wu, H., Chim, S.M., Zhou, L., Zhao, J., Feng, H., Wei, Q., Wang, Q., Zheng, M.H., Tan, R.X., et al. (2013). SC-514, a selective inhibitor of IKKβ attenuates RANKL-induced osteoclastogenesis and NF-κB activation. Biochem. Pharmacol. *86*, 1775–1783.
42. Lee, W.S., Lee, E.G., Sung, M.S., Choi, Y.J., and Yoo, W.H. (2018). Atorvastatin inhibits osteoclast differentiation by suppressing NF-κB and MAPK signaling during IL-1β-induced osteoclastogenesis. Korean J. Intern. Med. *33*, 397–406.
43. Xiao, F., Zuo, B., Tao, B., Wang, C., Li, Y., Peng, J., Shen, C., Cui, Y., Zhu, J., and Chen, X. (2021). Exosomes derived from cyclic mechanical stretch-exposed bone marrow mesenchymal stem cells inhibit RANKL-induced osteoclastogenesis through the NF-κB signaling pathway. Ann. Transl. Med. *9*, 798.
44. Ling, L., Murali, S., Stein, G.S., van Wijnen, A.J., and Cool, S.M. (2010). Glycosaminoglycans modulate RANKL-induced osteoclastogenesis. J. Cell. Biochem. *109*, 1222–1231.
45. Lee, S.I., Boyle, D.L., Berdeja, A., and Firestein, G.S. (2012). Regulation of inflammatory arthritis by the upstream kinase mitogen activated protein kinase kinase 7 in the c-Jun N-terminal kinase pathway. Arthritis Res. Ther. *14*, R38.
46. Matsumoto, M., Sudo, T., Saito, T., Osada, H., and Tsujimoto, M. (2000). Involvement of p38 mitogen-activated protein kinase signaling pathway in osteoclastogenesis mediated by receptor activator of NF-kappa B ligand (RANKL). J. Biol. Chem. *275*, 31155–31161.
47. Kim, B.H., Oh, J.H., and Lee, N.K. (2017). The Inactivation of ERK1/2, p38 and NF-kB Is Involved in the Down-Regulation of Osteoclastogenesis and Function by A2B Adenosine Receptor Stimulation. Mol. Cells *40*, 752–760.
48. Ihn, H.J., Kim, J.A., Lim, S., Nam, S.H., Hwang, S.H., Lim, J., Kim, G.Y., Choi, Y.H., Jeon, Y.J., Lee, B.J., et al. (2019). Fermented Oyster Extract Prevents Ovariectomy-Induced Bone Loss and Suppresses Osteoclastogenesis. Nutrients *11*, 1392.
49. Su, X.D., Yang, S.Y., Shrestha, S.K., and Soh, Y. (2022). Aster saponin A(2) inhibits osteoclastogenesis through mitogen-activated protein kinase-c-Fos-NFATc1 signaling pathway. J. Vet. Sci. *23*, e47.
50. Han, S.Y., Kim, J.H., Jo, E.H., and Kim, Y.K. (2021). Eleutherococcus sessiliflorus Inhibits Receptor Activator of Nuclear Factor Kappa-B Ligand (RANKL)-Induced Osteoclast Differentiation and Prevents Ovariectomy (OVX)-Induced Bone Loss. Molecules *26*, 1886.
51. Chiou, W.F., Huang, Y.L., and Liu, Y.W. (2014). (+)-Vitisin A inhibits osteoclast differentiation by preventing TRAF6 ubiquitination and TRAF6-TAK1 formation to suppress NFATc1 activation. PLoS One *9*, e89159.
52. Ihn, H.J., Lee, D., Lee, T., Kim, S.H., Shin, H.I., Bae, Y.C., Hong, J.M., and Park, E.K. (2015). Inhibitory Effects of KP-A159, a Thiazolopyridine Derivative, on Osteoclast Differentiation, Function, and Inflammatory Bone Loss via Suppression of RANKL-Induced MAP Kinase Signaling Pathway. PLoS One *10*, e0142201.
53. Huang, X.L., Liu, C., Shi, X.M., Cheng, Y.T., Zhou, Q., Li, J.P., and Liao, J. (2022). Zoledronic acid inhibits osteoclastogenesis and bone resorptive function by suppressing RANKL-mediated NF-κB and JNK and their downstream signalling pathways. Mol. Med. Rep. *25*, 59.
54. Tan, Y., Ke, M., Li, Z., Chen, Y., Zheng, J., Wang, Y., Zhou, X., Huang, G., and Li, X. (2021). A Nitrobenzoyl Sesquiterpenoid Insulicolide A Prevents Osteoclast Formation via Suppressing c-Fos-NFATc1 Signaling Pathway. Front. Pharmacol. *12*, 753240.
55. Okada, H., Okabe, K., and Tanaka, S. (2020). Finely-Tuned Calcium Oscillations in Osteoclast Differentiation and Bone Resorption. Int. J. Mol. Sci. *22*, 180.
56. Kito, H., and Ohya, S. (2021). Role of K(+) and Ca(2+)-Permeable Channels in Osteoblast Functions. Int. J. Mol. Sci. *22*, 10459.
57. Li, S., Yang, B., Teguh, D., Zhou, L., Xu, J., and Rong, L. (2016). Amyloid β Peptide Enhances RANKL-Induced Osteoclast Activation through NF-κB, ERK, and Calcium Oscillation Signaling. Int. J. Mol. Sci. *17*, 1683.
58. Chen, K., Yuan, Y., Wang, Z., Song, D., Zhao, J., Cao, Z., Chen, J., Guo, Q., Chen, L., Tickner, J., and Xu, J. (2019). Helvolic acid attenuates osteoclast formation and function via suppressing RANKL-induced NFATc1 activation. J. Cell. Physiol. *234*, 6477–6488.

STAR★METHODS

KEY RESOURCES TABLE

REAGENT or RESOURCE	SOURCE	IDENTIFIER
Antibodies		
NFATc1 antibody	Santa Cruz	Cat# sc-7294; RRID:AB_2152503
CTSK antibody	Santa Cruz	Cat# sc-48353; RRID:AB_2087687
P65 antibody	Santa Cruz	Cat# sc-8008 Alexa Fluor® 546; RRID:AB_628017
c-Fos antibody	Abcam	Cat# ab134122; RRID:AB_2848208
ATP6V0D2 antibody	Abcam	Cat# ab236375
β-actin antibody	Abcam	Cat# ab6276; RRID:AB_2223210
JNK antibody	Cell Signaling Technology	Cat# 9252; RRID:AB_2250373
p-JNK antibody	Cell Signaling Technology	Cat# 4668; RRID:AB_823588
P65 antibody	Cell Signaling Technology	Cat# 8242; RRID:AB_10859369
p-P65 antibody	Cell Signaling Technology	Cat# 3033; RRID:AB_331284
IκBα antibody	Cell Signaling Technology	Cat# 4812; RRID:AB_10694416
ERK antibody	Cell Signaling Technology	Cat# 4695; RRID:AB_390779
p-ERK antibody	Cell Signaling Technology	Cat# 4370; RRID:AB_2315112
p38 antibody	Cell Signaling Technology	Cat# 8690; RRID:AB_10999090
p-P38 antibody	Cell Signaling Technology	Cat# 4511; RRID:AB_2139682
Secondary antibodies	Thermo Fisher Scientific	Cat# SA535571; RRID:AB_2556775, Cat# SA535521; RRID:AB_2556774
Biological samples		
Murine bone marrow isolates	Guangxi Key Laboratory of Regenerative Medicine	N/A
Chemicals, peptides, and recombinant proteins		
CGK733 (CG)	Med Chem Express	CAS: 905973-89-9
DMSO	Solarbio	D8371
α-MEM	Thermo Fisher Scientific	12561–056
FBS	Thermo Fisher Scientific	10099141 C
P/S	Thermo Fisher Scientific	15140–122
RANKL	R&D Biotechnology	462-TEC-500
M-CSF	R&D Biotechnology	416-mL-500
PFA	Solarbio	P1110
E_2	Solarbio	E8140
PBS	Solarbio	P1020
BSA	Solarbio	A8020
Triton X-100	Solarbio	T8200
DAPI	Solarbio	C0065
Trizol	Thermo Fisher Scientific	15596018
SYBR Green Master	Roche	04913914001
Fluo-4, AM	Thermo Fisher Scientific	F14201
RIPA	Sigma-Aldrich	R0010
Loading buffer	Beyotime	P0015L
DMEM	Thermo Fisher Scientific	11054–001
Tribromoethanol	Nanjing Aibei Biotechnology	M2910

(*Continued on next page*)

Continued

REAGENT or RESOURCE	SOURCE	IDENTIFIER
Critical commercial assays		
Cell Counting Kit-8	Med Chem Express	Cat. No.: HY-K0301
Reverse transcription kits	Thermo Fisher Scientific	01182505
Alkaline Phosphatase Assay Kit	Beyotime Biotechnology	C3206
Annexin-V-FITC Apoptosis Detection Kit	BD Biosciences Pharmingen	556547
Mouse CTX-I ELISA Kit	Sangon Biotech	D721204
Experimental models: Cell line		
MC3T3-E1	Fuheng Biology	FH0384
Experimental models: Organisms/strains		
C57BL/6J mouse	Guangxi Medical University's experimental animal	N/A
Oligonucleotides		
Primers for qPCR, refer to Table S1	This paper	N/A
Software and algorithms		
ImageJ	National Institutes of Health	https://imagej.net/
GraphPad Prism 9	GraphPad	http://www.graphpad.com/

RESOURCE AVAILABILITY

Lead contact

Requests for further information, reagents and resources may be directed to our lead contact, Qian Liu (liuqian@gxmu.edu.cn).

Materials availability

This study did not generate new unique reagents.

Data and code availability

- Data: All data used to generate the figures in this manuscript and supplemental information will be shared by the lead contact upon request.
- Code: This study does not report original code.
- Additional information: Any additional information required to reanalyze the data reported in this paper is available from the lead contact upon request.

EXPERIMENTAL MODEL AND STUDY PARTICIPANT DETAILS

Animals

The C57BL/6J mice used in this study were purchased from Guangxi Medical University. 6-week-old C57BL/6J female mice were the source of bone marrow macrophages *in vitro*. 10-week-old C57BL/6J female mice were used in the OVX mouse model *in vivo*. All experimental procedures for the mouse study were carried out in accordance with the Guangxi Medical University Laboratory Animal Care Protocol and by the Animal Care and Welfare Committee. (SYXK 2020-0004, 202103048).

Bone marrow macrophages extraction

BMMs were isolated from the tibias and femurs of six-week-old C57BL/6J female mice and were the target cells of our *in vitro* experiment. The mice were firstly executed by cervical dislocation, and the tibias and femurs were disinfected with 75% alcohol before being stripped to remove other surrounding soft tissues. Bone marrow cells were flushed from the tibial and femoral medullary cavities. The cells were then cultured in α-MEM medium containing 10% fetal bovine serum, 1% penicillin/streptomycin and 25 ng/mL M-CSF at 37°C and 5% CO_2 for 3 days to obtain BMMs.

OVX model

The 10-week-old C57BL/6J female mice were randomly divided into 5 groups. After anesthesia, bilateral ovariectomy was performed to establish the OVX model. The ovaries of the sham-operated group were exposed and returned. After one week of recovery, the mice in each group underwent intraperitoneal injection of the corresponding drugs.

METHOD DETAILS

Materials and reagents

CGK733 was acquired from MedChemExpress (MCE, Shanghai, China) at 98% purity, dissolved in dimethyl sulfoxide (DMSO) to 20 mM, and diluted to 100 μM in α-MEM. The purchase of MC3T3-E1 was made at Fuheng Biology Company (Shanghai, China). Gibco (Thermo Fisher Biotechnology Institute, MD, USA) provided the alpha modification minimum necessary penicillin/streptomycin (P/S), alpha-modified minimal essential medium (α-MEM) and fetal bovine serum (FBS). M-CSF and RANKL came from R&D Biotechnology Company (Minneapolis, MN, USA). MedChemExpress (MCE, Shanghai, China) provided the Cell Counting Kit-8 (CCK-8). Thermo Fisher Biotechnology (Shanghai, China) supplied reverse transcription kits and immunoblotting test reagents. Alkaline Phosphatase Assay Kit was given by Beyotime Biotechnology (Shanghai, China). β-Estradiol (E_2) was given by Solarbio (Beijing, China). Santa Cruz Biotechnology provided NFATc1 (sc-7294), CTSK (sc-48353) and fluorescent antibodies for P65 (#sc-8008 Alexa Fluor 546) (Dallas, CA, United States). Abcam offered c-Fos (ab134122), ATP6V0D2 (ab236375) and β-actin (ab6276) (Cambridge, United Kingdom). JNK (#9252), *p*-JNK (#4668), P65 (#8242), p-P65 (#3033), IκBα (#4812), ERK (#4695), *p*-ERK (#4370), p38 (#8690) and p-P38 (#4511) were all specific primary antibodies obtained from Cell Signaling Technology (United States; Boston suburb).

Animal ethics

All experimental procedures for mouse studies were carried out in accordance with Guangxi Medical University's experimental animal care regulations and were approved by the Animal Care and Welfare Committee (SYXK 2020-0004, 202103048).

Cell culture

6-week-old C57BL/6J mice were utilized to separate bone marrow macrophages (BMMs). The tibia and femur bone marrow were extracted using a sterile syringe of 1 mL, and bone marrow macrophages (BMMs) were then cultured at 37°C in 5% CO_2 with complete medium and M-CSF at a concentration of 25 (ng/mL). After 48 h, the media was once again changed, and the final follow-up experiments were performed using adherent cells.

Cytotoxicity assay

In 96-well plates, 8×10^3 BMMs were seeded into each well. The next day, the cells were subjected to CG at a variety of concentrations, ranging from 0 to 6 μM, and they were then cultured for 96 h. A multimode microplate reader was used to analyze the absorbance at 450 nm (Biotek, United States) of each well 2 h after 10 μL CCK-8 was added. Annexin-V-FITC Apoptosis Detection Kit was applied to evaluate CG-induced apoptosis. BMMs were seeded into 6-well plates, incubated for 24 h to allow cell apposition, and then treated with CG (0, 3, 6 μM) for 48 h. The cells were then digested, cleaned, and resuspended before being incubated with FITC-labeled Annexin V and PI for 15 min and analyzed by flow cytometry (Becton, Dickinson and Company, United States).

Osteoclastogenesis assay

BMMs were seeded in 96-well plates at a density of 8×10^3 BMMs per well with α-MEM complete medium containing M-CSF. 24 h later, cells were stimulated by RANKL (50 ng/mL) with or without CG (0, 1, 2, 3, 4, 5 or 6 μM) treatment. BMMs were refed by the above medium every 2 days to ensure the growth of mature osteoclasts. Six days later, cells were fixed with 4% paraformaldehyde (PFA) for 50 min, rinsed with Phosphate buffer saline (PBS), and followed by tartrate-resistant acid phosphatase (TRAP) staining. Finally, taking 3 images for each group at 4× magnification was carried out by BioTek (Winooski, United States). To further explore the timeliness effect of CG in the various stages of osteoclast formation, RANKL-activated BMMs were treated with CG at a concentration of 6 μM throughout the early (1–3 days), middle (3–5 days) and late (5–7 days) differentiation phases. On day 7, cells were collected, and then PFA fixation, TRAP staining and image acquisition were conducted as the above method.

Podosome belt staining

To examine podosome belt development, BMMs were seeded into 96-well plates with a density of 8×10^3 cells/well. Twenty-four hours later, cells were treated with CG in varied concentrations (3, 6 μM) and refed every two days until mature osteoclasts were discovered on the 6^{th} day. These mature osteoclasts were fixed for 30 min with 4% PFA and permeabilized for 10 min with 0.1% Triton X-100, then sealed for 1 h with 3% bovine serum albumin (BSA)-PBS. Following rinsing three times with 0.2% BSA-PBS, rhodamine-phalloidin (1:500) was added to stain for 1 h, followed by 4,6-diamidino-2-phenylindole (DAPI) diluted with 0.2% BSA-PBS for 5 min. Cells were photographed with a BioTek microscope after being washed three times in PBS. ImageJ and GraphPad Prism were used for image quantitative and statistical analyses.

Immunofluorescence staining

The nuclear localization of P65 after RANKL stimulation was observed by fluorescence microscopy. BMMs were seeded on microscope petri plates overnight for adherence, starved for 3 h in serum-free media, and then activated by RANKL (50 ng/mL) for 30 min after being pre-stimulated for 1 h with or without 6 μM CG. These cells were first fixed in 4% PFA for 15 min, and then 0.1% Triton X-100 was used to penetrate them for an additional 5 min. Non-specific binding sites were blocked for 30 min with 3% BSA-PBS. Three times with 0.2% BSA-PBS washes were

followed by adding the fluorescent primary antibody of P65 and incubating at 4°C overnight. The nuclei were stained for 5 min with DAPI at 1:1000 in 0.2% BSA-PBS. Finally, images were taken using a BioTek microscope.

Bone resorption assay

The treated bone sections were placed flat on the bottom of a 96-well plate, and BMMs (1×10^4) were added to the well plate until the cells stuck to the bone sections or bottom.

Cells were stimulated with RANKL-containing medium until mature osteoclasts were detected in control wells, then CG (6 μM)-containing medium was added. After 2 days, control wells were fixed with 4% PFA and bone mini-slices were fixed with Electron microscope fixative solution. Finally, electron microscopy is used to scan the extent of resorption pits in bone slices.

Intracellular calcium (Ca^{2+}) oscillation assay

Calcium fluorophore Fluo4 was used to monitor calcium oscillation.[58] After seeding 1×10^4 BMMs onto 96-well plates, we incubated them with RANKL (50 ng/mL) and M-CSF (25 ng/mL) for 24 h in the presence or absence of 6 μM CG. After that, the cells were washed twice with assay buffer (consisting of 1x HANKS balanced salt solution, 100 mM probenecid, and 1% FBS), and then they were incubated for 45 min with 4 μM Fluo4 staining solution (consisting of Fluo4-AM dissolved in 20% Pluronic-F127 diluted in DMSO (w/v). After two washes with assay buffer, samples were observed using a fluorescence microscope (Bioteck) set to 488 nm excitation wavelength for 3 min while taking pictures at 2 s intervals and analyzing them in ImageJ. Change in oscillation intensity was calculated by first determining the minimum intensity and then comparing it to the greatest peak intensity.

Relative quantitative PCR (qPCR)

BMMs were grown at a concentration of 1.5×10^5 cells per well in 6-well plates and subsequently treated for 6 days with 50 ng/mL RANKL, either with or without CG. Total RNA was isolated from BMM-derived osteoclasts utilizing Trizol reagent (Thermo Fisher Scientific). RNA was converted to complementary DNA (cDNA) using a commercial reverse transcription kit, and the cDNA was then used as a qPCR sample. The qPCR was conducted using a LightCycler 96 System manufactured by Roche (Switzerland). The analysis was done with the $2^{-\Delta\Delta Ct}$ method, and the mean value of the target gene was computed using the cycle threshold (CT) value of β-actin as the reference. Table S1 displays the precise primer sequences that were used.

Western blot assay

In 6-well plates, BMMs (2×10^5 per well) were treated with or without CG (6 μM). to lyse the treated cells, radioimmunoprecipitation (RIPA) lysis buffer was used for 30 min at 4°C. The cell suspension was collected and centrifuged at 12000 rpm for 10 min at 4°C, the supernatant discarded, the loading buffer added, and the mixture heated for 15 min at 100°C. Electrophoretically separating the proteins using SDS-polyacrylamide gels (SDS-PAGE) and transferring them to nitrocellulose (NC) membranes was the next step. The non-specific binding sites were sealed with 5% skim milk for 1 h, then rinsed three times with Tris-Buffered Saline Tween 20 (TBST) before adding the primary antibody (1:1000) and shaking overnight at 4°C. Following a three-time TBST wash, the membrane was incubated for 1 h at room temperature with the secondary antibody. Finally, an infrared imaging system was used to scan and image the film. The grayscale value of protein bands was measured with ImageJ.

Osteoporotic ovariectomized (OVX) model mice

The Guangxi Medical University Animal Protection Committee has given its approval to all live animal experiments. Forty C57BL/6J mice (female, 10 weeks old) were randomly split into five groups (n = 8 per group): Sham + vehicle, OVX + vehicle, OVX + CG (3 mg/kg), OVX + CG (6 mg/kg), and OVX + E_2 (100 ng/kg). Bilateral ovariectomy mimicked postmenopausal osteoporosis after 1.25% Tribromoethanol anesthesia. The sham-operated mice, on the other hand, had their skin removed but their ovaries left intact. After one week following surgery, mice in the sham + Vehicle and OVX + Vehicle groups were injected intraperitoneally with 1% DMSO in saline, while the group of drug intervention was injected with 3 mg/kg and 6 mg/kg of CG, and OVX + E_2 group was injected intraperitoneally with 100 ng/kg E_2, every two days for 6 weeks. After 42 days, the femurs of all the mice were removed after they were killed through cervical dislocation so that they could be scanned with a micro-CT and analyzed histologically.

Micro-computed tomography (Micro-CT)

Each sample of bone tissue underwent a scan using an SCANCO Medical Micro-CT 50 equipment (SCANCO Medical, Switzerland). The scanning parameters were set as follows: source voltage 50 kV, source current 500 μA, 0.5 mm Al filter; The pixel size 9 μm; 180° rotation step. The left proximal femoral bone was chosen as the region of interest, and a 3D reconstruction was carried out using analog 19.0. The Skysacn CT program was used to examine many metrics of bone tissue, including the bone volume/tissue volume (BV/TV), the trabecular separation (Tb.Sp), the trabecular number (Tb. N), and the trabecular thickness (Tb.Th).

Histological assessment

The left femur was scanned using Micro-CT, decalcified at 37°C for two weeks, fixed in paraffin, and sectioned at a thickness of 5 μm. Hematoxylin and eosin (H&E) or TRAP staining was then performed on these sections. The hearts, livers, and kidneys of mice were similarly pretreated before H&E staining. In the meantime, immunohistochemical staining was utilized to detect CTSK expression. Using an orthomosaic microscope, images were magnified and acquired using ImageJ analysis software.

Differentiation of osteoblast precursor

After being thawed, MC3T3-E1 cells were cultured on T-75 cell culture plates using DMEM supplemented with 10% FBS and 1% P/S. When the cells had settled to cover 95% of the flask bottom, they were digested with DMEM for 3 min before being centrifuged at 1500 rpm for 5 min. Following the counting of the cells, 5×10^4 cells were seeded into each well of the 48-well plate. MC3T3-E1 cells were cultured in osteogenic induction medium containing DMEM,10 mM β-glycerophosphate, 50 μg/mL ascorbic acid and 10 nM dexamethasone, and treated with CG (0, 3, and 6 μM). The medium was changed every two days. After 7 days of culture, these cells were fixed with 4% PFA and stained for ALP. Cystatin 5 was used for image acquisition, and ImageJ was utilized for analysis.

ELISA assay

After collecting the ocular blood from the aforementioned animal model mice rest at room temperature for 1h, it was centrifuged at 4 °C at 1000 rpm for 20 min. The supernatant was subsequently used in further experiments. The concentration of serum C-terminal cross-linking telopeptide of type I collagen (CTX-1) was measured with the use of an ELISA kit (Sangon Biotech, Shanghai, China), which was used following the instructions provided by the manufacturer. After obtaining the optical density (OD) value of every well using a Multimode Microplate Reader set to 450 nm, the data was analyzed with GraphPad Prism 9.0.

QUANTIFICATION AND STATISTICAL ANALYSIS

The experimental data acquired in this research were taken from three or more duplicate trials and were presented as mean ± standard deviation (SD). GraphPad Prism 9 (Software, Inc., USA) was used to statistically analyze the data. The data were compared using one/two-way ANOVA. P-values less than 0.05 were deemed statistically significant.